Resonant and non-resonant inelastic x-ray scattering



2001 J. Phys.: Condens. Matter 13 7539

(http://iopscience.iop.org/0953-8984/13/34/306)

INSTITUTE OF PHYSICS PUBLISHING JOURNAL OF PHYSICS: CONDENSED MATTER

J. Phys.: Condens. Matter **13** (2001) 7539–7555 PII: S0953-8984(01)24204-0

# Resonant and non-resonant inelastic x-ray scattering

**K Hämäläinen and S Manninen**

Department of Physics, POB 64, University of Helsinki, FIN-00014 Helsinki, Finland

Received 24 April 2001
Published 9 August 2001
Online at stacks.iop.org/JPhysCM/13/7539

**Abstract**

Due to the rapid development in the instrumentation at the synchrotron radiation facilities, inelastic x-ray scattering has become a widely used tool in the studies of condensed matter during the past decade. Intense and tunable radiation with specific polarization properties has made it possible to study subtle details in the ground and the excited states of the electronic systems. One of the major strengths of the inelastic scattering technique is the possibility of controlling both the energy and the momentum transfers. In this paper a brief theoretical introduction to inelastic x-ray scattering is given and recent experimental results are presented and reviewed.

## 1. Introduction

Inelastic scattering of x-rays can be utilized in a wide range of experimental techniques to probe both the ground- and the excited-state properties of atoms, liquids and solids. Theoretically the starting point for describing the scattering process is the interaction of the electromagnetic field and the target electron. The non-relativistic interaction Hamiltonian can be written as

$$H_{int} = \sum_j \frac{e^2}{2mc^2} \boldsymbol{A}_j^2 + \sum_j \frac{e}{mc} \boldsymbol{p}_j \cdot \boldsymbol{A}_j \tag{1}$$

where $\boldsymbol{p}_j$ is the momentum of the $j$th target electron and $\boldsymbol{A}_j$ the vector potential of the electromagnetic field. The $\boldsymbol{A}^2$ term is responsible for scattering (including diffraction and non-resonant inelastic scattering), whereas $\boldsymbol{p} \cdot \boldsymbol{A}$ is related to the absorption processes and resonant scattering. Depending on the energy and the momentum transfer in the inelastic scattering process, quite distinct information can be obtained. Based on the high-resolution crystal spectrometers operating at the second- and third-generation synchrotron facilities, completely new possibilities have opened up in this field. Even meV-range excitations, such as phonons, are now accessible using x-rays. Study of various electronic excitations is possible with resolution of a few eV; however, this is two orders better than what is obtainable with conventional solid-state detectors. The relevant problems within the low-momentum-transfer regime include plasmons and unoccupied-state properties of various types. In the region of large energy and momentum transfer, ground-state properties including magnetic aspects can be probed using Compton scattering.

0953-8984/01/347539+17$30.00  

The second term in the interaction Hamiltonian (1) sets the framework for x-ray absorption spectroscopy. The x-ray absorption near-edge structure (XANES) and extended x-ray absorption fine structure (EXAFS) yield information on the density of unoccupied states and the local structure. Similar information can be obtained using resonant inelastic x-ray scattering (RIXS). In this case the incident photon is absorbed and a fluorescence is measured as a function of incident energy. In terms of the cross section derived from the interaction Hamiltonian, given by equation (1), this means that the $\boldsymbol{p}\cdot\boldsymbol{A}$ term should be treated within second-order perturbation theory.

The expression for the differential scattering cross section for inelastic x-ray scattering can be found in many textbooks and it is known as the Kramers–Heisenberg formula (Kramers and Heisenberg 1925):

$$\frac{\mathrm{d}^2\sigma}{\mathrm{d}\Omega\,\mathrm{d}\omega_2} = r_0^2\left(\frac{\omega_2}{\omega_1}\right)\sum_b\left|(\boldsymbol{e}_1\cdot\boldsymbol{e}_2)\langle b|\sum_j \mathrm{e}^{-\mathrm{i}\boldsymbol{k}\cdot\boldsymbol{r}_j}|a\rangle + \frac{1}{m}\sum_i\left[\frac{\langle b|\sum_j(\boldsymbol{e}_2\cdot\boldsymbol{p}_j)\mathrm{e}^{\mathrm{i}\boldsymbol{k}_2\cdot\boldsymbol{r}_j}|i\rangle\langle i|\sum_j(\boldsymbol{e}_1\cdot\boldsymbol{p}_j)\mathrm{e}^{-\mathrm{i}\boldsymbol{k}_1\cdot\boldsymbol{r}_j}|a\rangle}{E_a - E_i + \hbar\omega_1 + \mathrm{i}\Gamma/2} + \frac{\langle b|(\boldsymbol{e}_1\cdot\boldsymbol{p})\mathrm{e}^{-\mathrm{i}\boldsymbol{k}_1\cdot\boldsymbol{r}}|i\rangle\langle i|(\boldsymbol{e}_2\cdot\boldsymbol{p})\mathrm{e}^{\mathrm{i}\boldsymbol{k}_2\cdot\boldsymbol{r}}|a\rangle}{E_a - E_i - \hbar\omega_2 + \mathrm{i}\Gamma/2}\right]\right|^2\delta\left(\frac{E_b - E_a}{\hbar} - \omega\right) \tag{2}$$

where $\hbar\omega_1$ and $\hbar\omega_2$ are the incident and scattered photon energies, $\boldsymbol{k}_1$ and $\boldsymbol{k}_2$ the wave vectors of the incident and scattered photons and $\boldsymbol{e}_1$ and $\boldsymbol{e}_2$ the corresponding unit polarization vectors, respectively. The momentum transfer $\boldsymbol{k} = \boldsymbol{k}_1 - \boldsymbol{k}_2$. The electronic states involved in the transition are denoted as $|a\rangle$ (initial state), $|i\rangle$ (intermediate state) and $|b\rangle$ (final state), where $E_a$, $E_i$ and $E_b$ are the corresponding energies. The lifetime $\Gamma$ of the excited state appears as a result of time-dependent perturbation theory. The energy difference between the incident and scattered photon is denoted by $\hbar\omega$. The first term in equation (2) comes from the $\boldsymbol{A}^2$ contribution whereas the last two are related to the $\boldsymbol{p}\cdot\boldsymbol{A}$ term of the interaction Hamiltonian.

## 2. Non-resonant scattering

### *2.1. Theory*

The non-resonant scattering process is described by the first term in the Kramers–Heisenberg formula (2)

$$\frac{\mathrm{d}^2\sigma}{\mathrm{d}\Omega\,\mathrm{d}\omega_2} = r_0^2\left(\frac{\omega_2}{\omega_1}\right)\left|(\boldsymbol{e}_1\cdot\boldsymbol{e}_2)^2\sum_b\langle b|\sum_j \mathrm{e}^{-\mathrm{i}\boldsymbol{k}\cdot\boldsymbol{r}_j}|a\rangle\right|^2\delta\left(\frac{E_b - E_a}{\hbar} - \omega\right) \tag{3}$$

which is often written in the form

$$\frac{\mathrm{d}^2\sigma}{\mathrm{d}\Omega\,\mathrm{d}\omega_2} = r_0^2(\boldsymbol{e}_1\cdot\boldsymbol{e}_2)^2\left(\frac{\omega_2}{\omega_1}\right)S(\boldsymbol{k},\omega) \tag{4}$$

where $S(\boldsymbol{k},\omega)$ is the dynamic structure factor. It is important to notice that now the cross section is factorized in such a way that all the information on the target system is in the dynamic structure factor, which describes the response of the system to an external electromagnetic field.

Depending on the momentum and energy transfers there are different types of non-resonant inelastic x-ray scattering experiment, based on:

(i) *Compton scattering*, $kr_c \gg 1$, $\hbar\omega \gg E_B$, where $r_c$ is the inter-particle distance and $E_B$ the binding energy of the electron;
(ii) *valence electron excitations*, $kr_c \simeq 1$, $\omega/\omega_p \simeq 1$, where $\hbar\omega_p$ is the plasmon energy;

(iii) *inner-shell excitations*, $\hbar\omega \simeq E_B$, where $a$ is the inner-shell radius. If additionally $ka < 1$, one can apply the dipole approximation and relate the scattering cross section to the x-ray absorption spectra.

Also scattering from phonons takes place but it is not discussed in detail in this article.

One should note that the $\boldsymbol{A}^2$ term can be completely eliminated through the $(\boldsymbol{e}_1 \cdot \boldsymbol{e}_2)$ term if linearly polarized radiation and a scattering angle of 90° are used in the experiment at the plane of the linear polarization. This is a tool often used at synchrotron laboratories—where the radiation is naturally linearly polarized—for studying the $\boldsymbol{p} \cdot \boldsymbol{A}$ contribution to the Kramers–Heisenberg cross section.

### 2.2. Compton scattering

In the Compton scattering regime the dynamic scattering factor is considered in more detail.

The traditional idea of treating Compton scattering as a collision between a photon and a stationary free electron gives the well-known result for the wavelength shift

$$\Delta\lambda = \frac{e}{mc}(1 - \cos\theta)$$

where $\theta$ is the scattering angle. It is easy to introduce the effect of a moving electron using a semiclassical approach and writing the energy and momentum conservation laws as

$$\hbar\omega_1 + \frac{\boldsymbol{p}_1^2}{2m} = \hbar\omega_2 + \frac{\boldsymbol{p}_2^2}{2m} \tag{5}$$

$$\hbar\boldsymbol{k}_1 + \boldsymbol{p}_1 = \hbar\boldsymbol{k}_2 + \boldsymbol{p}_2. \tag{6}$$

Writing the energy transfer as $\hbar\omega = \hbar\omega_1 - \hbar\omega_2$ and the scattering vector as $\boldsymbol{k} = \boldsymbol{k}_2 - \boldsymbol{k}_1$ one obtains

$$\hbar\omega = \frac{(\hbar\boldsymbol{k})^2}{2m} - \frac{\hbar}{m}\boldsymbol{p}_1 \cdot \boldsymbol{k}. \tag{7}$$

The first term describes the Compton shift whereas the second term is determined by the component of the electron momentum along the scattering vector direction. Using this technique it is then possible to obtain a one-dimensional projection of the electron momentum density.

To treat the Compton scattering process more precisely the dynamic scattering factor, given in equations (3), (4), should be used. When the energy transferred to the electron in the inelastic scattering process is much larger than the electronic binding energies, the final-state wave function can be described by a plane wave $\mathrm{e}^{\boldsymbol{p}_2\cdot\boldsymbol{r}/\hbar}$. Additionally if the time of the scattering process is short, the potential energy cancels out for the initial and final states. This is called the *impulse approximation* (Eisenberger and Platzman 1970). Assuming Slater-determinant-type wave functions the dynamic scattering factor can then be written as

$$S_j(\boldsymbol{k},\omega) = \frac{1}{V}\left|\int \mathrm{d}^3\boldsymbol{r}\ \mathrm{e}^{-\mathrm{i}\boldsymbol{k}\cdot\boldsymbol{r}}\mathrm{e}^{-\mathrm{i}\boldsymbol{p}_2\cdot\boldsymbol{r}/\hbar}\varphi_j\right|^2 \delta\left(\omega - \frac{\hbar k^2}{2m} + \frac{\boldsymbol{p}_1\cdot\boldsymbol{k}}{m}\right) \tag{8}$$

where $\varphi_j(\boldsymbol{r})$ is the $j$th-electron initial-state wave function. According to equation (6) $\boldsymbol{p}_2 = \boldsymbol{p}_1 - \hbar\boldsymbol{k}$ and therefore the integral in equation (8) simply contains the Fourier transform of the ground-state wave function $\varphi_j$, i.e. the momentum-space wave function $\chi_j(\boldsymbol{p}_1)$. The $\delta$-function in equation (8) guarantees total-energy conservation. Adding contributions of all electrons $j$ in the target and writing $\rho(\boldsymbol{p}_1) = \sum_j |\chi_j(\boldsymbol{p}_1)|^2$, equation (8) gives

$$S(\boldsymbol{k},\omega) = \int \rho(\boldsymbol{p}_1)\,\mathrm{d}\boldsymbol{p}_1\,\delta\left(\omega - \frac{\hbar k^2}{2m} + \frac{\boldsymbol{p}_1\cdot\boldsymbol{k}}{m}\right). \tag{9}$$

If the direction of the scattering vector $\boldsymbol{k}$ is chosen to be along the $z$-axis, the $\delta$-function fixes only the component $p_z$ and the integration is over a constant-$p_z$ plane. At this Compton limit the dynamic scattering factor is called the Compton profile $J(p_z)$:

$$J(p_z) = \int\int \rho(\boldsymbol{p}_1)\,\mathrm{d}p_x\,\mathrm{d}p_y \tag{10}$$

and the scattering cross section (3) can be then written in a simple form:

$$\frac{\mathrm{d}^2\sigma}{\mathrm{d}\Omega\,\mathrm{d}\omega_2} = (\boldsymbol{e}_1\cdot\boldsymbol{e}_2)^2 r_0^2 \frac{m}{|\boldsymbol{k}|}\left(\frac{\omega_2}{\omega_1}\right) J(p_z). \tag{11}$$

This result is extremely useful for two reasons:

(i) It connects the measured scattering cross section directly to the electronic ground-state wave functions and therefore offers a straightforward way to compare the theory and the experiment.

(ii) The valence electron contribution, which is of primary interest in most cases, is located close to the peak of the Compton profile and could therefore be easily separated from the broad contribution of the core electrons. This is complementary to x-ray diffraction where the valence electron contribution at the position of the first Bragg peak can be very small, whereas it is clearly seen in the Compton profile.

In the following text some typical examples, based on recent experimental and theoretical results for Compton scattering, are given. An extended review containing more detailed treatment of the inelastic x-ray scattering theory has been given by Schülke (1991).

*2.2.1. Free-electron gas.* Due to the improved momentum-space resolution a special interest in Compton scattering spectroscopy has recently been directed towards *metals*. In addition to the basic feature of a metal, the Fermi surface, effects like electron–electron correlation and post-collision effects can now be studied using Compton scattering.

The starting point for describing the valence electrons in a metal is a non-interacting electron gas. The electron states are all occupied up to the maximum energy, the Fermi energy (see figure 1, later), and the momentum distribution is then

$$\rho(p) = \text{constant} = \frac{N}{\frac{4}{3}\pi p_F^3} \qquad \text{for } p \leqslant p_F \tag{12}$$

where $N$ is the number of free electrons per site and $p_F$ is the Fermi momentum. Above $p_F$ the momentum density is zero. Additionally the momentum distribution is now isotropic and equation (10) can be integrated over $p_x$ and $p_y$ giving

$$J(p_z) = 2\pi \int_{p_z}^{\infty} \mathrm{d}p\ \rho(p)p. \tag{13}$$

Substituting $\rho(p)$ from (12) gives

$$J(p_z) = \frac{3N}{4p_F^3}(p_F^2 - p_z^2). \tag{14}$$

The free-electron contribution to the Compton profile is then an inverted parabola including discontinuities of the first derivative at $\pm p_F$. The Fermi-surface topology could therefore be studied using this technique. The advantages of Compton scattering compared with alternative methods like those based on the de Haas–van Alphen effect or angular correlation of positron annihilation are: (i) measurements can be made at room temperature; and (ii) the quality requirements of single-crystal samples are not that severe. Extensive studies on Li and Be (Sakurai *et al* 1995, Huotari *et al* 2000) offer beautiful results on the Fermi-surface topology of these metals.

*2.2.2. Correlation effects.* Equation (12) is valid for a non-interacting free-electron gas at zero temperature. The discontinuity at $p = p_F$ is smeared at finite temperatures but this is a small effect which only slightly blurs the Fermi surface. A more important factor comes from the electron correlations which move some of the momentum density from below to above the Fermi momentum. The break in the occupation number still persists but gets renormalized to a smaller value $Z_F < 1$ (see figure 1, below). Several theoretical approaches for correlation in a homogeneous electron gas exist (Takada and Yasuhara 1991) and the experimentally determined renormalization parameter $Z_F$ is therefore an important factor for judging the correctness of those approaches. From the experimental point of view there is a severe problem due to the sharp break at the Fermi momentum. Any deconvolution method for removing the resolution effect fails at the break and an extremely good resolution is therefore required. Recent data on Li (Schülke *et al* 1996) and Al (Suortti *et al* 2000) exist, but the results are somewhat confusing. For Li $Z_F$ was considerably lower than the theoretical predictions whereas for Al the agreement was very close. It should be noted, however, that in order to extract $Z_F$ some fitting procedures were included and therefore further experiments with better statistics are required. A useful way to check various theoretical models is to use high pressure to change the free-electron density. The first attempt was made by Hämäläinen *et al* (2000b) by applying a pressure up to 42 kbar to a sodium sample. The induced changes in the momentum density were clearly seen in the measured Compton profiles, but the statistical accuracy was too low for one to make a quantitative comparison between various theories.

*2.2.3. Electron–ion interaction.* The experimental accuracy (both better statistics and resolution) obtained using the modern synchrotron radiation facilities makes it possible to study even finer details of the properties of the electrons in metals. In real metals the electron states can be described by Bloch orbitals which leads to the high-momentum components in the momentum distribution, shown schematically in figure 1. Only very few experimental results are available, although in principle such studies are important as a verification of the solid-state calculations. Oberli *et al* (1985) used the positron annihilation technique to observe high-momentum components in the [110] and [200] directions of Li and Na single crystals. Schülke *et al* (1996) measured eleven directional Compton profiles of Li and in the reconstructed momentum density they found the [110]-based high-momentum contribution. Huotari *et al* (2000, 2001b) were the first to make a direct observation of high-momentum components using inelastic x-ray scattering. They measured directional Compton profiles of Be and found a clear high-momentum signal in the valence electron contribution corresponding the [110] direction. The temperature dependence of this component was also studied and it turned out to be at the experimental detection limit.

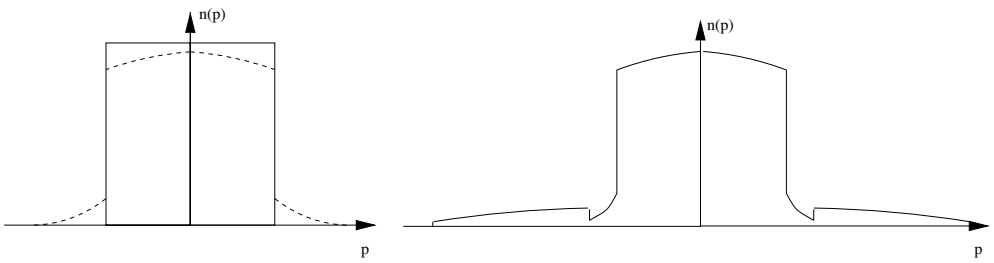


**Figure 1.** Left: the momentum density for a free-electron gas without (solid line) and with electron–electron correlation (dashed line). Right: the momentum density including the electron–ion interaction, which causes the high-momentum components above the Fermi momentum.

*2.2.4. Final-state effects.* A very important recent observation (although well known from the theoretical point of view) has been the effect of the so-called spectral density function describing the interaction between the ejected Compton electron and the other electrons in the system. In the first-order approximation the observed cross section is a convolution of the spectral density function and the Compton profile. In an extensive series of experiments on Li (Sakurai *et al* 1995) and Be (Huotari *et al* 2000) supported by theory (Sternemann *et al* 2000) it was shown that at the incident photon energies of the order of 10 keV, typical in high-resolution experiments, the resulting smearing crucially affects the resulting Compton scattering cross section. The effect is relatively small if higher photon energies are used. This ultimate limit of resolution is therefore an important fact in the design of inelastic x-ray scattering experiments.

*2.2.5. High-$T_C$ superconductors.* In addition to metals, a considerable effort in the field of inelastic x-ray scattering has been put into the studies of high-temperature superconductors. Both the ground-state electronic properties at room temperature and the true superconducting states have been investigated. Compared with alternative techniques, the real advantage is the insensitivity to crystal defects. On the other hand, all the electrons contribute to the scattered spectrum and therefore the interesting information from the valence electrons often overlaps with the core-electron contribution.

Manninen *et al* (1999) measured the Compton profiles of both powder and single-crystal samples $YBa_2Cu_3O_{7-\delta}$ and $Bi_2Sr_2CaCu_2O_8$ above and below the transition temperature to verify an earlier model and experimental result claiming a large temperature effect due to the electron rearrangement at the transition temperature. However, the observed effect was negligible both in the isotropic and in the directional profiles. Laukkanen *et al* (2001) performed an extensive experimental and theoretical study on the electronic properties of the $La_{1.85}Sr_{0.15}CuO_4$ system, which has served as a test case for both calculations and experimental techniques. The anisotropy between the [001] and [100] directions as well as the derivatives of the directional profiles were determined and compared with theoretical results obtained using an all-electron charge-self-consistent KKR model. The agreement between the experiment and the theory was good; small differences were explained by hybridization and weaker Fermi-surface-induced effects than anticipated by the theory.

Shukla *et al* (1999) made an interesting study on $PrBaCu_3O_{7-\delta}$ and $YBa_2Cu_3O_{7-\delta}$ crystals to explain why the former is an insulator but the latter a superconductor. Measuring directional Compton profiles and using a theoretical model based on full-potential augmented-plane-wave (FLAPW) calculations, they found that in $PrBaCu_3O_{7-\delta}$ the wave-function coherence was strongly suppressed compared to that in $YBa_2Cu_3O_{7-\delta}$.

*2.2.6. Chemical bonding.* The high-resolution Compton scattering technique has recently been extended to studies of the molecular bonding. Isaacs *et al* (1999) measured Compton profile anisotropies of ordinary ice to show that there is a substantial covalency of the hydrogen bond. Huotari *et al* (2000) have made an extensive series of Compton scattering experiments on simple molecules in gaseous and liquid form ($H_2O$, $N_2$). Comparing these results with those obtained for noble gases He and Ne, it was possible to accurately determine the contribution from the core electrons and concentrate on the effects originating from bonding.

*2.2.7. Magnetic Compton scattering.* Specific polarization properties of synchrotron radiation have made it possible to apply inelastic x-ray scattering in studies of magnetic properties of solids. The interaction between the electromagnetic field and the electron spin is weak and therefore neutrons have been a superior probe for magnetic properties. However,

the coupling between circularly polarized radiation and spin increases at high photon energies and this has been the motivation for magnetic Compton scattering experiments at high x-ray energies. Although synchrotron radiation is linearly polarized at the orbital plane, above and below that plane it becomes elliptically polarized. If one measures the Compton profile of a magnetized sample, changing the magnetization direction or the helicity of the radiation and taking the difference profile (the so-called magnetic Compton profile):

$$J_{mag}(p_z) = \int\int (n_\uparrow(\boldsymbol{p}) - n_\downarrow(\boldsymbol{p}))\,\mathrm{d}p_x\,\mathrm{d}p_y \tag{15}$$

the contribution of the core electrons cancels out and information about the momentum distribution of the unpaired spin electrons is obtained. Compared with the case for neutrons, the orbital component does not give any contribution to magnetic Compton scattering and therefore these two techniques are complementary. Measurements on all elemental ferromagnetic materials and several compounds have been made using this method (Cooper *et al* 1988, Duffy *et al* 1998) and photon energies even up to 1 MeV have been used (McCarthy *et al* 1997). Due to the intensity drop in the radiation extracted below or above the orbital plane of the electron orbit, alternative techniques for producing circularly polarized radiation for these experiments have been developed (Yamamoto *et al* 1989). These include elliptical multipole wigglers (Montano *et al* 2000) which operate at the orbital plane, and they will soon be routinely used at all third-generation synchrotron facilities.

Finally it should be noted that from measurements on the Compton electron in coincidence with the scattered photon, full three-dimensional information is obtained. This technique is called (x, ex) spectroscopy (or originally $(\gamma, \mathrm{e}\gamma)$ due to the gamma-ray sources used to produce high-energy photons). Although ideal in theory, the practical problems are the low counting rate, strong absorption and multiple scattering of the electrons. For these reasons, the (x, ex) technique is limited to application to very thin samples.

### *2.3. Plasmons*

The dynamic structure factor is related to several other fundamental quantities which reveal its importance in understanding the electronic structure and dynamics. Using the time-dependent formalism one can show that

$$S(\boldsymbol{k}, \omega) = \frac{1}{2\pi}\int \mathrm{d}t\ \mathrm{e}^{-\mathrm{i}\omega t}\langle n_{\boldsymbol{k}}(t) n_{-\boldsymbol{k}}(0)\rangle \tag{16}$$

so the dynamic structure factor is proportional to the Fourier transform of the density–density correlation function. Now it is easier to see that with small momentum transfer the long-range interaction effects are important and collective excitations can be studied. On the other hand, at large momentum transfer the independent-particle picture is valid as in the case of Compton scattering.

The importance of the dynamic structure factor is emphasized in the fluctuation-dissipation theorem:

$$S(\boldsymbol{k}, \omega) = -\frac{\hbar k^2}{4\pi^2 e^2 n}\,\mathrm{Im}\left[\frac{1}{\varepsilon(\boldsymbol{k}, \omega)}\right] \tag{17}$$

where $\varepsilon(\boldsymbol{k}, \omega)$ is the dielectric function which describes the response of the system to an electromagnetic field and strongly depends on the electronic structure. The dielectric function directly couples the electronic structure and macroscopic behaviour of the material since it is measurable via the reflectance and the refractive index, for example.

It can be shown in a simple semiclassical picture that in certain cases a free-electron gas responds collectively to an external electromagnetic field by oscillating at a fixed resonance frequency. These excitations, plasmons, are also observable in the inelastic scattering spectra at low momentum transfer. The momentum dispersion and lifetime effects of plasmon peaks are of fundamental interest in many-body theory. In a broader concept the plasmons are poles of a dielectric function and when proper calculations are accomplished these are coupled in a complicated way to the complete electronic system under study (see Schülke (2001), in this Special Issue). During the last decade several studies on the plasmon dispersion utilizing inelastic x-ray scattering have been accomplished on a broad range of materials.

### *2.4. Valence excitations*

One of the key features in the strength of inelastic x-ray scattering is the possibility of controlling both the energy and momentum transfer. A typical optical absorption spectrum carries information on the joint density of states when the valence electrons are excited to the unoccupied conduction band. In the process of inelastic scattering from a single-crystal sample one is able to choose both the direction and the amount of momentum transfer given to the system. Furthermore, the experiment can be done using hard x-rays and genuine bulk information can be obtained. Various single-crystal samples have been studied by this technique (Hill *et al* 1998, Sternemann *et al* 1998). One unique application is the possibility of studying the indirect band gaps, which has been very recently demonstrated in the case of diamond (Caliebe *et al* 2000).

### *2.5. Inner-electron excitations*

It can be shown that under certain approximations the inelastic scattering cross section is directly proportional to the absorption coefficient (Mizuno and Ohmura 1967). This is true for low-momentum-transfer excitations from inner-shell electrons and the scattering is often referred to as non-resonant Raman scattering. In the scattering case the direction of momentum transfer determines the reference coordinate system (as polarization does in the case of absorption) and directional information on local electronic structure comparable to that from XANES can be obtained (Schülke *et al* 1988, Manninen and Hämäläinen 1992). Even EXAFS oscillations are observable (Tohji and Udagawa 1989) which opens up a unique way to study low-lying absorption edges with penetrating x-rays. These include carbon and oxygen K edges which are of great importance in many biological systems and difficult to study with soft x-rays.

However, as in the case of the absorption process, the remaining hole can complicate the interpretation of the spectra. The simplest implications of the electron–hole interaction are the energy shifts which are well known in VUV spectroscopy. The inclusion of electron–hole interaction in the theory is not that straightforward but very recently a successful *ab initio* computational scheme has been introduced within the soft-x-ray (Benedict and Shirley 1999) and hard-x-ray (Soininen and Shirley 2000) regimes. The application to lithium fluoride (Caliebe *et al* 2000) clearly shows the importance of proper inclusion of final-state effects. The role of electron–hole interaction is even more striking in the case of inner-shell excitations, where clearly resolved exciton peaks can be observed. Figure 2 shows energy-loss spectra for the fluorine K edge in LiF. The anomalous intensity dependence of the pre-peak as a function of the momentum transfer clearly identifies it as an s-type exciton.

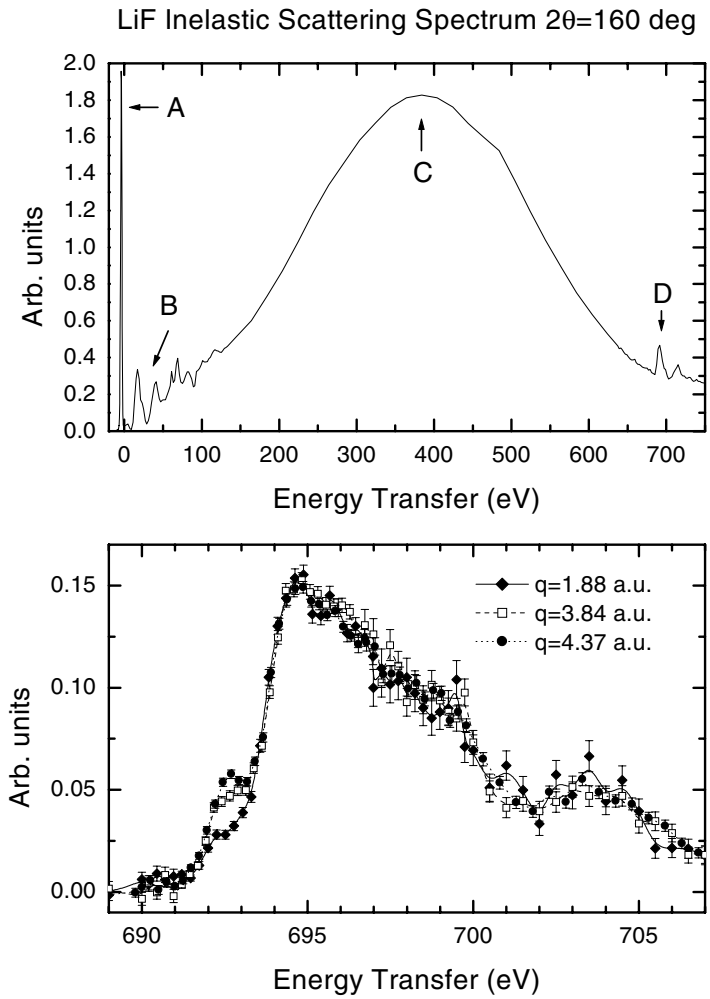


**Figure 2.** Top: the inelastic scattering spectrum as a function of the energy transfer for LiF measured at 10 keV. A: the quasielastic line representing the resolution function with FWHM of 1 eV; B: non-resonant scattering from lithium and fluorine valence electrons; C: the Compton profile of LiF, where the peak value represents the classical Compton shift; and D: the non-resonant inelastic scattering spectrum from fluorine K electrons. Bottom: more detailed spectra at the fluorine K edge (D in the top panel) for several momentum-transfer values indicated in the figure. The Compton background from other electrons is subtracted out and the data are normalized to the peak value. The pre-peak intensity shows non-dipole intensity dependence.

## 3. Resonant scattering

### *3.1. Absorption spectroscopy*

Besides diffraction, x-ray absorption spectroscopy is one of the most frequently used techniques utilizing synchrotron radiation. Its success is based on the use of one of the basic features of radiation from a bending magnet, namely the tunability of the incident energy. Furthermore, the actual experiment is rather straightforward: it simply consists in measuring the intensity loss at the sample as a function of energy. In the absorption process the incident photon ejects

an inner-shell electron, creating a core hole. Since the binding energy of the core electron is fixed, the variation of the incident energy is directly reflected (via the energy conservation principle) in the kinetic energy of the ejected photo-electron. The variation in the absorption cross section is then due to the changes in the transition probability, i.e. in the density of states and the transition matrix elements. This gives the possibility of gaining local structural information on the unoccupied electronic states by using the photo-electron as an indirect probe. However, the role of the core state is significant because

(i) it determines the atom under study (elemental specificity) and

(ii) the symmetry restrictions related to a chosen electron shell determine the allowed transitions (selection rules) and the probed partial density of states.

On the other hand, the deep core holes will decay very fast (the lifetime is of the order of $10^{-15}$ s) which will also create energy uncertainty and broaden the observed spectral features. This is referred to as lifetime broadening and fundamentally limits the applicability of near-edge absorption spectroscopy (XANES) in the study of small dynamical changes due to the chemical reactions, for example.

### *3.2. Emission spectroscopy*

One can also follow the absorption process one step further and measure the energy spectra of the emission lines following the core-hole decay (referred to as radiative decay). Quantum mechanically this can be described as a second-order process according to equation (2) where the core-hole + photo-electron state is the intermediate state. When the incident energy is well above the resonance (absorption edge), the energy and width of the emission line are determined by the energy levels and the corresponding lifetimes involved in the process. However, the total intensity of the emission line is modulated by the absorption probability, which offers an alternative way to measure the absorption cross section. This, the so-called fluorescence method, is frequently utilized in absorption spectroscopy when the samples are too thick to allow transmission measurements. However, some care has to taken that the sample self-absorption effects are properly included in the data analysis.

The typical widths of the emission lines in the hard-x-ray regime are of the order of a few eV and cannot be resolved without crystal spectrometers. However, such an energy analysis of the fluorescence lines can be done even with conventional x-ray sources. In this case (when the incident energy is scanned and is well above the absorption edge), the spectral shape of the emission line can bear valuable information on, for example, the multiplet splitting of the states involved in the transitions. The energy levels are normally rather deep lying and therefore it is mainly information on the occupied density of states that can be gained. However, when the final-state hole approaches the valence band, the sensitivity to chemical changes increases dramatically. K$\beta$ lines are already rather sensitive to the local electronic structure and can be used even with conventional sources for routine laboratory chemical analysis. An example for Ni is shown in figure 3. But only very recently, due to the advent of synchrotron radiation, has it become feasible to perform a true two-dimensional energy mapping of the emission lines, i.e. to measure the full energy spectrum of emission lines while tuning the incident energy in the vicinity of an absorption edge. It should be noticed that such a measurement cannot carry more information than is buried in a simple absorption spectrum. However, certain spectral features can be resolved and sometimes enhanced in this manner. In the following, some specific applications of this technique are discussed.

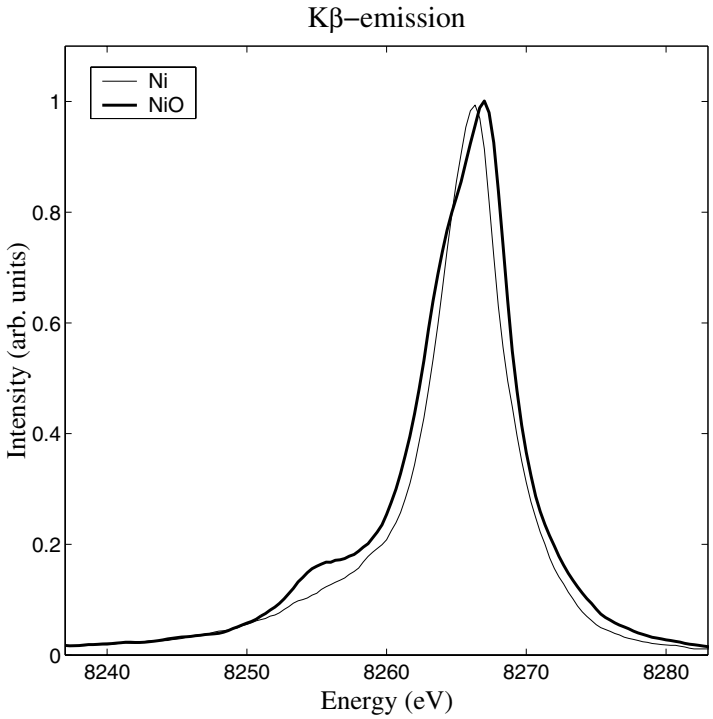


**Figure 3.** K$\beta$ emission spectra for Ni and NiO. The change of chemical environment is clearly seen in the shift of the peak position and in the shoulder structure.

### *3.3. Resonant Raman scattering*

As mentioned before, well above the absorption edge the position and the spectral shape of the emission line stay unchanged. However, when the incident energy is tuned in the vicinity of the absorption edge the behaviour dramatically changes. The position of the emission line exhibits a dispersion in position, the shape becomes highly asymmetric and the intensity is resonantly enhanced when the incident energy approaches the absorption edge. An example is shown in figure 4. This emission behaviour below the edge is referred to as resonant Raman scattering (RRS) and was first observed in the x-ray region by Sparks (1974). The process and the cross section can be well understood on the basis of the Kramers–Heisenberg formula (see for example Aberg and Tulkki 1985). Several moderate-resolution works have confirmed the calculated dispersion characteristics (Eisenberger *et al* 1976a, b) and even some applications to utilizing RRS in the determination of lifetime widths have been developed (Hämäläinen *et al* 1989).

### *3.4. Sub-lifetime spectroscopy*

If the intensity of a fluorescence line is monitored within a narrower energy bandwidth than its natural lifetime width while the incident energy is scanned though an absorption edge, a dramatic sharpening of the actual edge and the spectral shapes occurs. This was first demonstrated by Hämäläinen *et al* in the case of the dysprosium $L_{III}$ edge (Hämäläinen *et al* 1991). The observed anomaly is a simple consequence of the total-energy conservation principle and can be explained by second-order perturbation theory and the

Kramers–Heisenberg formula (2). As a result of high-resolution fluorescence monitoring, absorption spectrum features which are almost completely smeared by the lifetime broadening in the conventional transmission data can be resolved. This behaviour is easy to understand in a phenomenological one-electron, two-step picture (Hämäläinen *et al* 1989). It was later pointed out (Carra *et al* 1995) that in some cases the multi-electron interaction will change the corresponding energy levels and the fluorescence line can be shifted. Consequently the interpretation of such one-dimensional measurements is no longer that straightforward. Therefore, it is essential to collect first a complete two-dimensional data set and understand the overall behaviour of the emission line. After this, which is in most cases compulsory due to the count rate/measurement time restrictions, one can perform one-dimensional scans.

### *3.5. Discrete excitations*

Just below the actual absorption edge one can often observe so-called pre-peaks which are related to well-defined transitions to atomic-like or hybridized states. The nature of these weak spectral features is sometimes difficult to clarify because they are smeared by the lifetime broadening of the absorption edge. These peaks are clearly resolved when the high-resolution emission technique is employed, which has been nicely demonstrated for Dy 4f (Hämäläinen *et al* 1991) and Mn 3d (Hämäläinen *et al* 1992) localized states. Since in this case the energy of the photo-electron final state is well defined, the emission spectra show rather anomalous dispersion when the incident energy is scanned in the vicinity of these pre-peaks. Actually, it had already been pointed out by Heitler (1954) that in this case one can observe anomalously narrow (sub-lifetime) emission spectra. Furthermore, the emission spectra show clear resonance behaviour at fixed energy transfer which can be utilized to separate the discrete excitations from the continuous ones. Figure 4 demonstrates the clear difference between typical RRS and a discrete excitation. This was demonstrated in the case of Gd (Krisch *et al* 1995) and recently a more extensive work on series of rare-earth compounds has been accomplished (Bartolome *et al* 1999). These localized states are of a great importance as regards magnetic properties and a combined study with x-ray circular magnetic dichroism will give essential information on the underlying electronic structure.

### *3.6. Site selectivity*

Many structural probes, x-ray diffraction for example, are not especially sensitive to a change of chemical environment or the ionization state. EXAFS has elemental specificity but it will average over all the atoms of a certain $Z$ in the system under study regardless of their chemical state. The change of ionization state, however, can be observed in the absorption data as an energy shift of the edge. The change of the chemical state is also reflected in the other energy levels and can be seen in the positions and spectral shape of the corresponding emission lines. This is seen in figure 3 where the shift in the emission spectra between Ni metal and NiO is caused by the ionization of the Ni atom. The Mn K$\beta$ fluorescence line is another good example where systematic shifts in the peak position can be observed as a function of the oxidation state (Peng *et al* 1994). With a high-resolution spectrometer this gives the possibility of selectively choosing (or rather enhancing, since the various emission lines are still overlapping) the detection of a certain chemical state (Grush *et al* 1995). This technique has been extensively applied to various Mn compounds since the change of the oxidation state plays a crucial role in the photosynthesis cycle. Another useful application is to Mn- and Ni-based lithium-ion batteries where the chemical changes during the charging and discharging cycle can be monitored *in situ* (Mattila *et al* 2001).

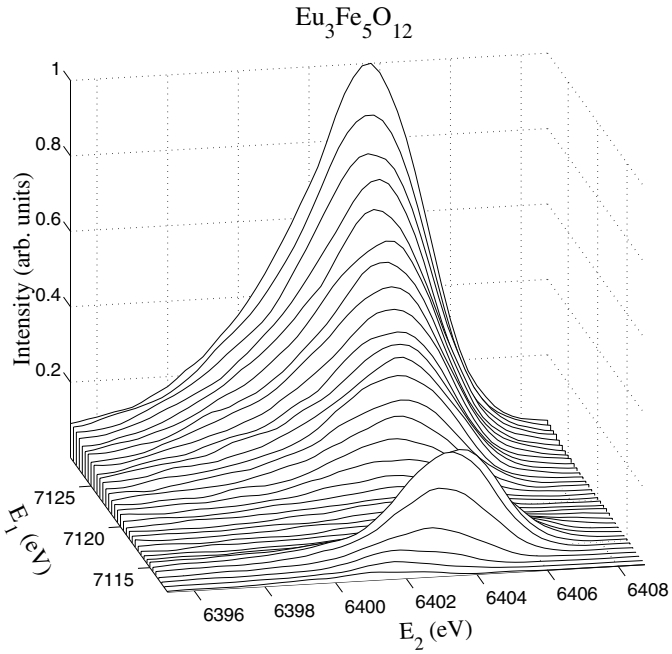


**Figure 4.** A two-dimensional resonant scattering scan of europium iron garnet, where the energy spectrum of scattered photons (energy $E_2$) is measured for several incident energies ($E_1$) in the vicinity of the europium $L_{III}$ absorption edge.

### *3.7. Spin selectivity*

The usefulness of the final-state selectivity strongly relies on the knowledge of the detailed structure of the emission line splitting. The Mn K$\beta$ emission line serves as an excellent example because it has a clear satellite peak almost 20 eV apart from the main line (deGroot *et al* 1995). Furthermore, it is well known that due to its peculiar 3d-electron configuration (in the neutral state, all spin-up states are occupied, while all spin-down states are empty according to Hund's rule), the main peak predominantly corresponds to a spin-up final-state hole while the satellite structure is due to the spin-down hole on the 3p shell after the emission process. Now by selectively monitoring only a specific decay channel, one is able to obtain spin-selective absorption spectra. This has been demonstrated for MnO and $MnF_2$ (Hämäläinen *et al* 1992). Remarkably in this case spin information from an antiferromagnetic system can be gained without any external magnetic field. Spin-configuration information relevant to the macroscopic magnetism can further be exploited by using circularly polarized incident radiation. This has been demonstrated using a helical undulator source to obtain circularly polarized hard x-rays in the case of Gd (Krisch *et al* 1996).

### *3.8. Multiple ionization*

Some of the observed satellite structures in the emission lines are due to the multi-ionization processes in the target atom. A systematic study of these weak processes via photo-excitation has become possible only due to synchrotron radiation. This provides valuable information on the atomic multiplet splitting and the possibility of scanning the incident energy has opened up totally new possibilities for studying the actual multi-ionization process (Deutsch *et al*

1996, Fritsch *et al* 1998). Recent studies include the creation of so-called hollow atoms with a completely empty K shell (Diamant *et al* 2000). Systematic study as a function of $Z$ also gives the possibility of examining the transition from $LS$- to $jj$-coupling (Diamant *et al* 2001).

### *3.9. Charge-transfer excitations*

Until very recently all the resonant inelastic scattering experiments have been concentrated, due to intensity and resolution limitations, on transitions where both the intermediate and the final states are localized. However, Kao *et al* (1996) have demonstrated in the case of NiO that transitions with energy losses of only few eV corresponding to the valence electron excitations also become observable when they are resonantly enhanced by tuning the incident energy in the vicinity of an absorption edge. Even with the most powerful insertion devices the observed resonances correspond to only a maximum of a few counts per second, so they are still far beyond the resonances observed in the case of magnetic elastic scattering (Isaacs *et al* 1989). The observed structure in the energy-loss data can be related to charge-transfer excitations. Similar resonant enhancement has been observed also in highly correlated electron systems, like high-$T_C$ superconductor precursor compounds with CuO planes (Hill *et al* 1998). These excitations can exhibit polarization dependence which can be understood via modern cluster calculations (Hämäläinen *et al* 2000a). The observed momentum-transfer dependencies are somewhat ambiguous for various systems and there are also suggestions that the observed resonances and momentum-transfer behaviour can only be explained by third-order phenomena (Abbamonte *et al* 1999). In such experiments the resonant behaviour enables use of an interesting and as yet unexploited technique to address the charge-transfer excitations with hard x-rays.

## 4. Instrumentation

The study of electronic excitations requires energy resolution of a few eV or better. This resolution is easily obtainable for the typical incident energy by normal single-crystal monochromators. However, energy analysis of the scattered photons with such a precision is not that straightforward and instead of conventional detectors crystal analysers must be used. Typical x-ray spectrometers for eV-resolution studies are based on curved crystals and simultaneously offer focusing characteristics. At present, mainly two alternatives, both based on the same principle of the Rowland-circle geometry, are utilized at various synchrotron radiation facilities.

*In the scanning crystal spectrometer* the sample, the analysing crystal and the detector are all on the focusing Roland circle. The energy spectrum of the scattered radiation is measured by scanning the analyser crystal through the desired Bragg angles. Both the analyser crystal and the detector move along the focusing circle during the scan. The resolution mostly depends on the size of the irradiated volume seen by the analyser crystal. At higher x-ray energies the incident beam energy bandwidth and the size and reflecting properties of the analyser crystal also become crucial. The uncertainty in the scattering angle due to the finite size of the analyser crystal can also significantly affect the momentum-space resolution, especially at lower x-ray energies (Hämäläinen *et al* 1996). Due to the scanning procedure it is important to monitor the incident beam intensity reliably. A scanning spectrometer suitable for use at high energies (mainly used for Compton scattering) has been operating at ESRF since its opening for public use (Suortti *et al* 1999). The momentum-space resolution depends on the incident energy and is about 0.15 au of momentum at 60 keV and 0.10 au at 30 keV.

The other possibility is to scan the incident energy while keeping the analyser part of the spectrometer at a fixed position (the so-called inverse-energy-scan method). This makes it

possible to use an extreme backscattering geometry in order to improve the energy resolution. Suitable spectrometers for this exist at HASYLAB (Schülke 1986)—this spectrometer also utilizes very effectively the so-called dispersion compensation, at NSLS (Hämäläinen *et al* 1997) and also at beamline ID16 at ESRF. The momentum-space resolution is as good as 0.02 au at 10 keV. The backscattering geometry combined with the possible choices of the analyser crystals limit this method to the x-ray regime below 15 keV only. Such spectrometers are also used for energy-loss and emission spectroscopies which require sub-eV resolution. The major limitation for resonance scattering experiments is the availability of suitable analyser crystals which would operate close to backscattering geometry for the desired energy regime. At the present time, major effort is being put into pushing the total-energy resolution down to 0.1 eV, which requires the use of four-bounce monochromators and diced analyser crystals.

*In the energy-dispersive spectrometer* the analyser crystal at the Rowland circle disperses the energy spectrum from the sample and a position-sensitive detector is then used to measure the spectral distribution. Since the original construction at LURE (Loupias and Petiau 1980) similar constructions have been made in Germany (Berthold *et al* 1992) and in Japan (Sakurai *et al* 1992). These spectrometers are mainly used for Compton scattering and the resolution is about 0.10–0.15 au of momentum depending on the incident energy and the geometrical details. The advantage of the dispersive method is that the whole energy spectrum is acquired simultaneously and no incident beam monitoring is required. On the other hand, when compared with the situation for scanning spectrometers, the background is much higher. Furthermore, the efficiency of the position-sensitive detector should be accurately known.

## 5. Summary and conclusions

In this paper we have given the basic framework for resonant and non-resonant inelastic x-ray scattering spectroscopy in the study of electronic structure and excitations. Several examples of recent works as well as advances are discussed. Since hard x-rays penetrate well into the sample, inelastic scattering offers a complementary method for studying the actual bulk-like properties which are not always that easily accessible with electrons or soft x-rays. Great potential can be seen in the high-pressure applications and *in situ* studies for vacuum-incompatible sample environments.

## Acknowledgments

The authors are indebted to all colleagues who have contributed to our work presented here, especially W Caliebe, J B Hastings and C-C Kao. We would also like to acknowledge S Galambosi, S Huotari, A Mattila and A Soininen for their valuable contribution to this publication. This work was supported by the Academy of Finland (7379/40732).

## References

Abbamonte P, Burns C A, Isaacs E D, Platzman P M, Miller L L, Cheong S W and Klein M V 1999 *Phys. Rev. Lett.* **83** 860

Aberg T and Tulkki J 1985 *Atomic and Inner-Shell Physics* (New York: Plenum) p 419

Bartolome F, Krisch M H, Raoux D and Tonnere J-M 1999 *Phys. Rev.* B **60** 13 497

Benedict L X and Shirley E L 1999 *Phys. Rev.* B **59** 5441

Berthold A, Mourikis S, Schmitz J R, Schülke W and Schulte-Schrepping H 1992 *Nucl. Instrum. Methods* **317** 373

Caliebe W A C, Soininen J A, Shirley E L, Kao C-C and Hämäläinen K 2000 *Phys. Rev. Lett.* **84** 3907

Carra P, Fabrizio M and Thole B T 1995 *Phys. Rev. Lett.* **74** 3700

Cooper M J, Collins S P, Timms D N, Brahmia A, Kane P P, Holt R S and Laundy D N 1988 *Nature* **333** 151

deGroot F M F, Pizzini S, Fontaine A, Hämäläinen K, Kao C-C and Hastings J B 1995 *Phys. Rev.* B **51** 1045
Deutsch M, Gang O, Hämäläinen K and Kao C-C 1996 *Phys. Rev. Lett.* **76** 2424
Diamant R, Huotari S, Hämäläinen K, Kao C-C and Deutsch M 2000 *Phys. Rev. Lett.* **84** 3278
Diamant R, Huotari S, Hämäläinen K, Kao C-C and Deutsch M 2001 *Phys. Rev.* A **62** 52519
Duffy J A, McCarthy J E, Dugdale S B, Honkimäki V, Cooper M J, Alam M A, Jarlborg T and Palmer S B 1998 *J. Phys.: Condens. Matter* **10** 10 391
Eisenberger P and Platzman P M 1970 *Phys. Rev* A **2** 415
Eisenberger P, Platzman P M and Winick H 1976a *Phys. Rev. Lett.* **36** 623
Eisenberger P, Platzman P M and Winick H 1976b *Phys. Rev.* B **13** 2377
Fritsch M, Kao C-C, Hämäläinen K, Gang O, Förster E and Deutsch M 1998 *Phys. Rev.* A **57** 1686
Grush M M, Christou G, Hämäläinen K and Cramer S P 1995 *J. Am. Chem. Soc.* **117** 5895
Heitler W 1954 *The Quantum Theory of Solids* (Oxford: Clarendon)
Hill J P, Kao C-C, Caliebe W, Matsubara M, Kotani A, Peng J L and Greene R L 1998 *Phys. Rev. Lett.* **80** 4967
Huotari S, Galambosi S, Hämäläinen K, Manninen S, Soininen A, Mattila A and Buslaps T 2001a to be published
Huotari S, Hämäläinen K, Manninen S, Kaprzyk S, Bansil A, Caliebe W, Buslaps T, Honkimäki V and Suortti P 2000 *Phys. Rev.* B **62** 7956
Huotari S, Hämäläinen K, Manninen S, Sternemann C, Kaprolat A, Schülke W and Buslaps T 2001b to be published
Hämäläinen K, Hill J P, Huotari S, Kao C-C, Berman L E, Kotani A, Ide T, Peng J L and Greene R L 2000a *Phys. Rev.* B **61** 1836
Hämäläinen K, Huotari S, Laukkanen J, Soininen A, Manninen S, Kao C-C, Buslaps T and Mezouar M 2000b *Phys. Rev.* B **62** R735
Hämäläinen K, Kao C-C, Hastings J B, Siddons D P, Berman L E, Stojanoff V and Cramer S P 1992 *Phys. Rev.* B **46** 14 274
Hämäläinen K, Manninen S, Caliebe W, Kao C-C and Hastings J B 1997 *AIP Conf. Proc.* **389** 671
Hämäläinen K, Manninen S, Kao C-C, Caliebe W, Hastings J B, Bansil A, Kaprzyk S and Platzman P M 1996 *Phys. Rev.* B **54** 5453
Hämäläinen K, Manninen S, Suortti P, Collins S P, Cooper M J and Laundy D 1989 *J. Phys.: Condens. Matter* **1** 5955
Hämäläinen K, Siddons D P, Hastings J B and Berman L E 1991 *Phys. Rev. Lett.* **67** 2850
Isaacs E, McWhan D B, Peters C, Ice G E, Siddons D P, Hastings J B, Vettier C and Vogt O 1989 *Phys. Rev. Lett.* **62** 1671
Isaacs E, Shukla A, Platzman P M, Hamann D R, Barbiellini B and Tulk C A 1999 *Phys. Rev. Lett.* **82** 600
Kao C-C, Caliebe W A L, Hastings J B and Gillet J-M 1996 *Phys. Rev.* B **54** 16 361
Kramers H A and Heisenberg W 1925 *Z. Phys.* **31** 681
Krisch M H, Kao C-C, Sette F, Caliebe W A, Hämäläinen K and Hastings J B 1995 *Phys. Rev. Lett.* **74** 4931
Krisch M H, Sette F, Bergmann U, Masciovecchio C, Verbeni R, Coulon J, Caliebe W and Kao C-C 1996 *Phys. Rev.* B **54** R12 673
Laukkanen J, Hämäläinen K, Manninen S, Shukla A, Bansil A, Kaprzyk S and Takashaki T 2001 *J. Phys. Chem. Solids* at press
Loupias G and Petiau J 1980 *J. Physique* **41** 265
Manninen S and Hämäläinen K 1992 *Phys. Rev.* B **45** 3878
Manninen S, Hämäläinen K, Dixon M A G, Cooper M, Cardwell D A and Buslaps T 1999 *Physica* C **314** 19
Mattila A *et al* 2001 unpublished
McCarthy J E, Cooper M J, Honkimäki V, Tschentscher T, Suortti P, Gardelis S, Hämäläinen K, Manninen S O and Timms D N 1997 *Nucl. Instrum. Methods* A **401** 563
Mizuno Y and Ohmura Y 1967 *J. Phys. Soc. Japan* **22** 445
Montano P A, Ruett U, Beno M A, Jennings G and Kimball C W 2000 *J. Phys. Chem. Solids* **61** 353
Oberli L, Manuel A A, Sachot R, Descouts P, Peter M, Rabou L P L M, Mijnarends P, Hyodo T and Stewart A T 1985 *Phys. Rev.* B **31** 1147
Peng G, deGroot F M F, Hämäläinen K, Moore J A, Wang X, Grush M M, Hastings J B, Siddons D P, Armstrong W H, Mullins O C and Cramer S P 1994 *J. Am. Phys. Soc.* **116** 2914
Sakurai Y, Ito M, Urai T, Tanaka Y, Sakai N, Iwazumi T, Kawata H, Ando M and Shiotani N 1992 *Rev. Sci. Instrum.* **63** 1190
Sakurai Y, Tanaka Y, Bansil A, Kaprzyk S, Stewart A T, Nagashima Y, Hyodo T, Nanao S, Kawata H and Shiotani N 1995 *Phys. Rev. Lett.* **74** 2252
Schülke W 1986 *Nucl. Instrum. Methods* A **246** 491
Schülke W 1991 *Handbook on Synchrotron Radiation* vol 3 (Amsterdam: North-Holland/American Elsevier) p 565
Schülke W 2001 *J. Phys.: Condens. Matter* **13**
Schülke W, Berthold A, Kaprolat A and Güntherodt H-J 1988 *Phys. Rev. Lett.* **60** 2217

Schülke W, Stutz G, Wohlert F and Kaprolat A 1996 *Phys. Rev.* B **54** 14 381
Shukla A, Barbiellini B, Erb A, Manuel A A, Buslaps T, Honkimäki V and Suortti P 1999 *Phys. Rev.* B **59** 12 127
Soininen J A and Shirley E L 2000 *Phys. Rev.* B **61** 16 423
Sparks C J 1974 *Phys. Rev. Lett.* **33** 262
Sternemann C, Hämäläinen K, Kaprolat A, Soininen A, Döring G, Kao C-C, Manninen S and Schülke W 2000 *Phys. Rev.* B **62** R7687
Sternemann C, Kaprolat A and Schülke W 1998 *Phys. Rev.* B **57** 622
Suortti P, Buslaps T, Fajardo P, Honkimäki V, Kretzschmer M, Lienert U, McCarthy J E, Renier M, Shukla A, Tschentscher T and Meinander T 1999 *J. Synchrotron Radiat.* **6** 69
Suortti P, Buslaps T, Honkimäki V, Metz C, Shukla A, Tschentscher T, Kwiatkowska J, Maniawski F, Bansil A, Kaprzyk S, Kheifets A S, Lun D R, Sattler T, Schneider J R and Bell F 2000 *J. Phys. Chem. Solids* **61** 397
Takada Y and Yasuhara H 1991 *Phys. Rev.* B **44** 7879 and references therein
Tohji K and Udagawa Y 1989 *Phys. Rev.* B **39** 7590
Yamamoto S, Kawata M, Kitamura H, Ando M, Sakai N and Shiotani N 1989 *Phys. Rev. Lett.* **62** 2672